Available online at www.sciencedirect.com
SCIENCE DIRECT
Chemical Physics 325 (2006) 499–508
Chemical Physics
www.elsevier.com/locate/chemphys

First infrared spectroscopic characterization of digermyl (Ge_2H_5) and d5-digermyl (Ge_2D_5) radicals in low temperature germane matrices

William Carrier [a], Weijun Zheng [a,b], Yoshihiro Osamura [c], Ralf I. Kaiser [a,*]

[a] Department of Chemistry, University of Hawai'i at Manoa, 255 The Mall, Honolulu, HI 96822, USA
[b] Institute for Astronomy, University of Hawai'i at Manoa, Honolulu, HI 96822, USA
[c] Department of Chemistry, Rikkyo University, 3-34-1 Nishi-ikebukuro, Tokyo, 171-8501, Japan

Received 12 September 2005; accepted 8 November 2005
Available online 20 February 2006

Abstract

The digermyl, $Ge_2H_5(X^2A')$ and d5-digermyl, $Ge_2D_5(X^2A')$, radicals were detected for the first time in low temperature germane and d4-germane matrices at 12 K via infrared spectroscopy after an irradiation of the samples with mono energetic electrons. Considering a scaling factor of 0.97, ab initio calculations showed that the most intense absorption of the digermyl radical should be observable for the ν_6 fundamental at 770 cm^{-1} $Ge_2H_5(X^2A')$ and 547 cm^{-1} $Ge_2D_5(X^2A')$, respectively. The actually experimental results (765 cm^{-1} and 561 cm^{-1}) are in good agreement with these computed data; we also detected the ν_4/ν_{12} mode of the d5-digermyl radical at 616 cm^{-1}. These data may aid in the monitoring of time resolved infrared spectroscopy of germane chemical vapor deposition processes and can also guide prospective observations of germanium-bearing molecules in the atmospheres of Jupiter and Saturn in the infrared regime to better understand the chemical evolution of planetary atmospheres under extreme environments.

1. Introduction

A detailed understanding of the structures, spectroscopic properties, and energetics of simple hydrogenated germanium clusters of the generic formula Ge_2H_x ($x = 1$–6) are of growing importance to technological applications such as germane chemical vapor deposition (CVD) and semiconductor processing [1–5]. Plasma etching processes, reactive plasma, and chemical vapor deposition techniques are of wide technological interest to produce germanium-bearing nano particles and amorphous germanium films (a-Ge:H) via microelectronic engineering [6,7]. Germanium films also have applications in material sciences, particularly in the development of solar cells, electro-photographic drums, and arrays for liquid crystal displays. In chemical vapor deposition processes, germane (GeH_4) or digermane (Ge_2H_6) precursor molecules are decomposed by hot filaments or electrons generated within plasmas [8,9]. During this process, germanium bearing species such as GeH_x ($x = 1$–3) and dinuclear clusters like Ge_2H_x ($x = 1$–5) have been identified in the gas phase as major growth species to produce amorphous, often porous germanium films.

The routes of formation and properties of the digermyl radical, $Ge_2H_5(X^2A')$, have recently attracted great interest in the growing semiconductor industry due to its use as a precursor in chemical vapor deposition processes [10]. A theoretical investigation on $Ge_2H_5(X^2A')$ [1] suggested that a $Ge_2H_4(X^1A_g)$ molecule combines with a hydrogen atom (reaction (1)). The reaction exoergicity to form the digermyl radical was calculated to be 237 kJ mol^{-1}. A second formation route was found to proceed through digermane, $Ge_2H_6(X^1A_{1g})$. An excitation from the ground state can either lead to a germanium-germanium (reaction (2)) or germanium-hydrogen bond rupture (reaction (3)). The reaction endoergicities were computed to be 271 kJ mol^{-1} and 330 kJ mol^{-1}, respectively.

$$Ge_2H_4(X^1A_g) + H(^2S_{1/2}) \rightarrow Ge_2H_5(X^2A') \quad (1)$$

* Corresponding author. Tel.: +1 808 956 5731; fax: +1 808 956 5908.
E-mail address: kaiser@gold.chem.hawaii.edu (R.I. Kaiser).

0301-0104/$ - see front matter © 2006 Elsevier B.V. All rights reserved.
doi:10.1016/j.chemphys.2005.11.046

$$Ge_2H_6(X^1A_{1g}) \rightarrow 2\ GeH_3(X^2A_1) \quad (2)$$

$$Ge_2H_6(X^1A_{1g}) \rightarrow Ge_2H_5(X^2A')+H(^2S_{1/2}) \quad (3)$$

Note that germane CVD processes modeled via complex reaction networks also require an in depth knowledge of the underlying chemical mechanisms. Currently, in situ characterization of gaseous molecules in CVD processes is predominantly carried out via mass spectrometry [11–13], but this technique can hardly discriminate between structural isomers; furthermore, lacking the fragmentation pattern of these germanium-bearing molecules makes it difficult to observe the corresponding radicals. To provide input to CVD reaction networks, a systematic study of the thermochemical properties and adiabatic ionization potentials of the germanium hydrides was performed very recently [10]. However, despite the importance of the Ge_2H_x ($x = 1$–6) species in chemical vapor deposition processes of germane, no time resolved spectroscopic probes such as infrared spectroscopy have been established – predominantly because only limited information on the infrared absorptions of these species are available. A few vibrational spectra of Ge_2H_x ($x = 2,4,6$) have been reported [14–17]; the most intense infrared absorptions of digermane, $Ge_2H_6(X^1A_{1g})$ [ν_6 and ν_8; 752 cm^{-1} and 881 cm^{-1}], a Ge_2H_4 isomer [789 cm^{-1}], and the di-bridged $Ge_2H_2(X^1A_1)$ [ν_6; 972 cm^{-1}] have been experimentally observed in low temperature neon matrices [15]. Surprisingly, data on the corresponding radical species ($x = 1,3,5$) have not previously been recorded.

In this paper we present, through a focused experimental and computational approach, our investigation for the vibrational levels of digermyl radicals $Ge_2H_5(X^2A')$ and their deuterated isotopomers in low temperature matrices. We have demonstrated earlier that an interaction of energetic electrons can cleave a carbon–hydrogen bond in a methane molecule to form atomic hydrogen and a methyl radical at 10 K (reaction (4)) [18]. Two neighboring methyl radicals were found to recombine forming an ethane molecule (Eq. (5)). Upon further irradiation with electrons, the ethane molecule decomposes to a hydrogen atom plus an ethyl radical (Eq. (6)). Our research group utilized a similar approach to characterize the infrared absorptions of the hitherto unknown disilyl, $Si_2H_5(X^2A')$ [19] and disilenyl, H_2SiSiH (X^2A), radicals [20] together with their perdeuterated isotopomers in low temperature silane matrices via the reaction sequence (7)–(9). Here, we expand this protocol and synthesize the digermyl radical via a homologous reaction sequence in germane and d4-germane matrices [21–23], reactions (10) and (11).

$$CH_4(X^1A_1) \rightarrow CH_3(X^2A_2'') + H(^2S_{1/2}) \quad (4)$$

$$CH_3(X^2A_2'') + CH_3(X^2A_2'') \rightarrow C_2H_6(X^1A_{1g}) \quad (5)$$

$$C_2H_6(X^1A_{1g}) \rightarrow C_2H_5(X^2A')+H(^2S_{1/2}) \quad (6)$$

$$SiH_4(X^1A_1) \rightarrow SiH_3(X^2A_1)+H(^2S_{1/2}) \quad (7)$$

$$SiH_3(X^2A_1)+SiH_3(X^2A_1) \rightarrow Si_2H_6(X^1A_{1g}) \quad (8)$$

$$Si_2H_6(X^1A_{1g}) \rightarrow Si_2H_5(X^2A') \rightarrow H_3SiSiH(X^1A')/H_2SiSiH_2(X^1A_g) \rightarrow H_2SiSiH(X^2A) \quad (9)$$

$$GeH_4(X^1A_1) \rightarrow GeH_3(X^2A_1)+H(^2S_{1/2}) \quad (10)$$

$$GeH_3(X^2A_1) + GeH_3(X^2A_1) \rightarrow Ge_2H_6(X^1A_{1g}) \quad (11)$$

$$Ge_2H_6(X^1A_{1g}) \rightarrow Ge_2H_5(X^2A') \quad (12)$$

By combining our experiments with electronic structure calculations, we provide information not only on the vibrational levels of elusive Ge_2H_5 and Ge_2D_5 radicals, but also on their geometries and enthalpies of formation. An exact understanding of the energetics allows the refinement of existing CVD reaction networks which model the formation of amorphous germanium films. Finally, the infrared data provides guidance towards the search for dinuclear germanium clusters in the atmospheres of Jupiter and Saturn. Here, the germane molecule (GeH_4) – a potential precursor to complex organo germanium molecules – has been observed spectroscopically with relative abundance of 7×10^{-10} and 4×10^{-10} relative to hydrogen, respectively [24]. Achieving a better understanding of the main Group IV organometallic chemistry along with the properties of multiple bonds and their energetics will therefore provide a better understanding to the origin and evolution of the atmospheres of the giant gas planets [25,27–31].

2. Experimental

The experiments were performed in a ultrahigh vacuum (UHV) machine [28]. Its main chamber can be evacuated down to 5×10^{-11} Torr by a magnetically suspended turbo pump backed by an oil-free scroll pump. A rotatable closed cycle helium refrigerator; is attached to the main chamber and holds a polished silver mirror. The silver mirror can be cooled to 10 K and serves as a substrate for the ice condensate. Gas samples can be brought into the chamber through a precision leak valve, which is connected to a gas reservoir and supported by a linear transfer mechanism. During the gas condensation, the deposition system can be moved to 5 mm in front of the silver mirror. This setup guarantees a reproducible thickness of the ice samples. The germane ices were prepared at 12 K by depositing germane (99.99%) and d4-germane (99.99%) at pressures of about 7×10^{-8} Torr for 30 min onto the cooled silver mirror. Fig. 1 shows a infrared absorption spectrum of germane ice.

These ices were irradiated at 12 K with 5 keV electrons generated with an electron gun at beam currents of 10 nA, 100 nA and 1000 nA. The irradiation was carried out for 60 min by scanning the ice over an area of 3.0 ± 0.4 cm^2. Using a Fourier transform infrared spectrometer (FT-IR) and a quadrupole mass spectrometer (QMS) guarantees identification of the reaction products in the solid state and gas phase, respectively. A background analysis was performed by collecting data with no germane

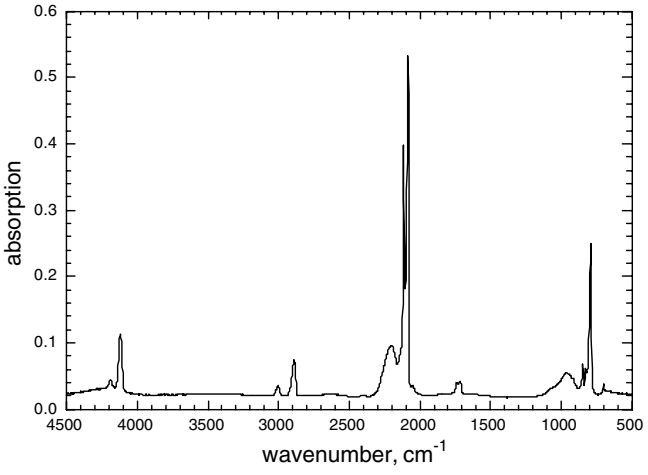

Fig. 1. Infrared spectrum of the germane frost at 12 K; absorptions are compiled in Table 1.

Table 1
Infrared absorptions of the germane (left column) and d4-germane (center column) frosts (sh: shoulder); α, β, and γ denote lattice modes of the germane sample

Frequency (cm^{-1})	Frequency (cm^{-1})	Assignment
4190	3002	$2\nu_3$
4120	2889	$\nu_1 + \nu_3$
3025	2172	$\nu_2 + \nu_3 + \alpha$
3000	2156	$\nu_2 + \nu_3$
2200	1597	$\nu_3 + \gamma$
2140	1543	$\nu_3 + \beta$
2114	1524	$\nu_3 + \alpha$
1737	1247	$\nu_2 + \nu_4 + \alpha$
1715	1231	$\nu_2 + \nu_4$
958	681	$\nu_4 + \gamma$
914	652	ν_2
846	616	$\nu_4 + \beta$
826	598	$\nu_4 + \alpha$
790	574	ν_4

in the UHV chamber. The Nicolet 510 DX FT-IR machine (5000–500 cm^{-1}) operated in an absorption-reflection-absorption mode (reflection angle $\alpha = 75°$) (resolution 0.5–2 cm^{-1}). The infrared beam was coupled via a mirror flipper outside the spectrometer, passed through a differentially pumped potassium bromide (KBr) window, was attenuated in the ice sample prior to and after reflection at a polished silver wafer, and exited the main chamber through a second differentially pumped KBr window before being monitored via a liquid nitrogen cooled detector. The gas phase is monitored via the Balzer QMG 420 (1–200 amu mass range) operating with electron impact ionization of the neutral molecules in the residual gas analyzer mode at electron energies of 100 eV and photomultiplier running at 200V. The dwell time of the masses was chosen to be 0.5 ms.

We would like to comment briefly on the phase of the solid germane ice. Solid GeH_4 has been spectroscopically observed in low temperatures crystals revealing α, β, and γ lattice modes [21]. The phases I–IV of germane can be discriminated easily via infrared spectroscopy of the ν_1–ν_3 and ν_2–ν_4 regions [35]. These data suggest a germane phase III in our experiment. We can also determine the thickness of the sample via the integrated infrared absorption features at 2111 and 821 cm^{-1}. The ice thickness was then calculated using the Lambert–Beer relationship [18]. The integrated absorption coefficients of these fundamentals, 5.5×10^{-17} and 4.7×10^{-17} cm mol^{-1}, respectively, and the density of the germane ice 1.751 g cm^{-3} [33] determined an optical thickness of 54 ± 20 nm (see Table 1).

3. Theoretical approach

The molecular structures and vibrational frequencies of the GeH_x species ($x = 1$–4) as well as digermane (Ge_2H_6) and digermyl molecules (Ge_2H_5) together with their perdeuterated species were scrutinized in terms of ab initio molecular orbital methods. The geometries were optimized with the hybrid density functional B3LYP method, i.e., Becke's three-parameter non-local exchange functional [36] with the non-local correlation functional of Lee, Yang, and Parr [37] and the 6-311G(d,p) basis set [38]. Since the energy of the quartet electronic state of the Ge_2H_5 radicals are extremely high and dissociative, we have only studied the doublet electronic state. We have examined various isomeric structures of Ge_2H_5 species for mono-bridged, di-bridged, and tri-bridged geometries in addition to the H_3GeGeH_2 structure in analogy to the Si_2H_5 system [20]. All optimized geometries with di-bridged and tri-bridged structures are shown to have more than two imaginary frequencies and they turned into either two structures when we optimized further along each imaginary mode. The vibrational frequencies and infrared intensities were obtained for optimized GeH_x ($x = 1$–4) and Ge_2H_x ($x = 5$, 6) species and the deuterated isotopomers. The coupled cluster CCSD(T) calculations [39,40] with the aug-cc-pVDZ basis set [41] were also conducted at the optimized structures obtained with the B3LYP method in order to compare the relative energies for the systems. All computations were carried out using the GAUSSIAN-98 program package [42]. The relative energies stated in the text are corrected with the zero-point vibrational energies obtained with the B3LYP method.

4. Computational results

The most stable structure of Ge_2H_6 molecule is the staggered conformation similar to ethane (C_2H_6) and disilane (Si_2H_6) as shown in Fig. 2(a). The rotational barrier of GeH_3 group in Ge_2H_6 is very small (2.2 kJ mol^{-1}) due to the long Ge–Ge bond distance (2.445 Å). This energy barrier is much smaller than those of ethane (10.2 kJ mol^{-1}) and disilane (3.2 kJ mol^{-1}) at the B3LYP level of theory. The second stable isomer of Ge_2H_6 species is the complex between a GeH_2 unit and germane (GeH_4) as shown in Fig. 2(b). The structure of this Ge_2H_6 isomer indicates that the vacant p-orbital of the GeH_2 moiety is acting as an

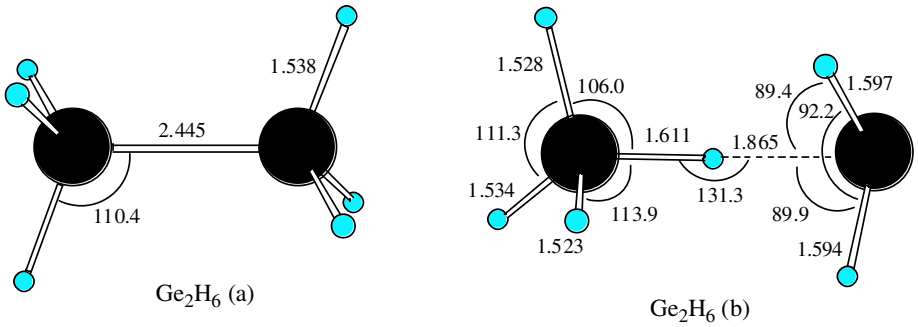

Fig. 2. Two isomeric structures of Ge_2H_6 calculated with the B3LYP/6-311G(d,p) method. Bond lengths and bond angles are in Å and °.

Table 2
Relative energies (kJ mol^{-1}) for Ge_2H_6 and Ge_2H_5 species at the B3LYP/6-311G(d,p) and CCSD(T)/aug-cc-pVDZ levels of theory

Species	B3LYP method (kJ mol^{-1})	CCSD(T) method (kJ mol^{-1})
$Ge_2H_6(X^1A_{1g})$ (a)	0.0	0.0
$Ge_2H_6(X^1A)$ (b)	137.8	142.5
$GeH_2(X^1A_1) + GeH_4(X^1A_1)$	158.4	172.1
2 $GeH_3(X^2A_1)$	266.8	271.3
Ge_2H_5(a) + H	334.0	329.7
$Ge_2H_5(X^2A')$ (a)	0.0	0.0
$Ge_2H_5(X^2A)$ (b)	91.4	92.9
GeH ($X^2\Pi$) + $GeH_4(X^1A_1)$	112.2	121.3
$GeH_2(X^1A_1) + GeH_3(X^2A_1)$	170.0	181.0

electron acceptor of the electrons of Ge–H bond in GeH_4. The energy of this complex is 142.5 kJ mol^{-1} higher than the energy of the most stable Ge_2H_6 isomer (a). The complexation energy from $GeH_2(X^1A_1)$ and $GeH_4(X^1A_1)$ is calculated to 29.6 kJ mol^{-1}. The relative energies and frequencies are summarized in Tables 2 and 3, respectively. Fig. 3 depicts two isomeric structures obtained for the Ge_2H_5 system. The most stable Ge_2H_5(a) structure is similar to ethyl radical whereas the least stable isomer Ge_2H_5 (b) resembles a complex between GeH and GeH_4 species. The structure Ge_2H_5 (b) is 92.9 kJ mol^{-1} less stable than the most stable Ge_2H_5(a). The complexation energy from GeH ($X^2\Pi$) and $GeH_4(X^1A_1)$ is calculated to 28.4 kJ mol^{-1}. This complex (b) is also observed in the case of Si_2H_5 system whose stabilization energy is very similar to the Ge_2H_5 system. The Ge–H bond dissociation energy to form the digermyl radical Ge_2H_5 plus atomic hydrogen from digermane was computed to be 329.7 kJ mol^{-1}. For completeness, we also investigated the structures (Fig. 4) and vibration frequencies of the GeH_x ($x = 1$–4) species and their deuterated counterparts (Table 4).

5. Experimental results

Infrared absorptions of the germyl radical, $GeH_3(X^2A_1)$, appeared instantaneously with the start of the irradiation of the germane sample with an electron current of 10 nA at 10 K at 665 cm^{-1} (Table 5; Fig. 5). The position of this ν_2 umbrella mode agrees well with previous experiments utilizing neon, deuterium, and argon gas matrices (663–667 cm^{-1}) [15]. The remaining two modes of the germyl radical, the ν_3 germanium-hydrogen stretch (2050–2093 cm^{-1}) and the ν_4 deformation mode (852–857 cm^{-1}) are obscured by the ν_3 and ν_4 fundamentals of the germane ice (Fig. 1). Therefore, these absorptions were not undeniably observed. Note that the absorptions of $GeH(X^2\Pi)$ and $GeH_2(X^1A_1)$ species were not detected in our investigation. Features of the digermane molecule, $Ge_2H_6(X^1A_{1g})$, also appeared immediately after the initiation of the irradiation (Fig. 6). We were able to observe an absorption at 752 cm^{-1}; this can be assigned to the ν_6 umbrella mode. The less intense deformation mode ν_{11} of the GeH_3 group is also observable at 870 cm^{-1} (see Fig. 7). Based on the integrated intensities, an intensity ratio of the absorption coefficients of the 752 cm^{-1} versus 870 cm^{-1} band was derived to be about 3.5 ± 0.5; this is in excellent agreement with the theoretically computed value (Table 3). Neither of the germanium-hydrogen stretching modes ν_5 or ν_{10} of the digermane molecule was observable due to the overlap of fundamentals with the germane species (Fig. 1; Table 1). The ν_{11} band of digermane was outside the range of our MCTB detector. Likewise, we were unable to detect the thermodynamically less stable second Ge_2H_6 isomer, H_3GeH–GeH_2 (Fig. 2; Table 1). Note that the assignments of the germyl radical and of the digermane molecule were cross checked in d4-germane matrices. Here, we detected the d3-germyl radical via its ν_4 mode at 608 cm^{-1} (Fig. 8) and also the d6-digermane molecule at 529 cm^{-1} (ν_6) and 626 cm^{-1} (ν_{11}) (Figs. 8 and 9). Summarized, at low irradiation times, absorptions of the germyl radical, $GeH_3(X^2A_1)$, and of the digermane molecule, $Ge_2H_6(X^1A_{1g})$, together with their deuterated counterparts can be observed unambiguously in the germane and d4-germane matrices (Table 5).

Having identified the germyl radical and the digermane molecule, we exposed the germane matrix to an enhanced irradiation time. The primary objective of this approach is to examine if the digermane molecule can also undergo a germanium-hydrogen bond rupture via Eq. (3) yielding the digermyl radical, $Ge_2H_5(X^2A')$. As a matter of fact, we were able to detect an additional absorption at 765 cm^{-1} (Table 5; Fig. 6). Accounting for a scaling factor

Table 3
Unscaled vibrational frequencies (cm^{-1}) and infrared intensities (cm $molecule^{-1}$) of Ge_2H_n and Ge_2D_n ($n = 5, 6$) calculated with B3LYP/6-311G(d,p) level of theory

Modes	Frequencies	Intensities	Frequencies	Intensities	Characterization
	Ge_2H_6(a)		Ge_2D_6(a)		$H_3GeGeH_3(X^1A_{1g})$
$\nu_1(a_{1g})$	2128	0	1509	0	GeH_3 symmetric stretch
$\nu_2(a_{1g})$	849	0	609	0	GeH_3 umbrella
$\nu_3(a_{1g})$	255	0	251	0	Ge–Ge stretch
$\nu_4(a_{1u})$	130	0	92	0	Torsion
$\nu_5(a_{2u})$	2122	2.64×10^{-17}	1504	1.39×10^{-17}	GeH_3 symmetric stretch
$\nu_6(a_{2u})$	766	8.40×10^{-17}	552	4.34×10^{-17}	GeH_3 umbrella
$\nu_7(e_g)$	2131	0	1519	0	GeH_3 asymmetric stretch
$\nu_8(e_g)$	891	0	632	0	GeH_3 deformation
$\nu_9(e_g)$	568	0	417	0	GeH_3 rock
$\nu_{10}(e_u)$	2141	7.97×10^{-17}	1527	4.16×10^{-17}	GeH_3 asymmetric stretch
$\nu_{11}(e_u)$	896	2.38×10^{-17}	638	1.21×10^{-17}	GeH_3 deformation
$\nu_{12}(e_u)$	374	6.43×10^{-18}	265	3.21×10^{-18}	GeH_3 rock
	Ge_2H_6 (b)		Ge_2D_6 (b)		$H_3GeH\cdots GeH_2(X^1A)$
ν_1(a)	2199	9.12×10^{-18}	1568	5.28×10^{-18}	GeH_3 asymmetric stretch
ν_2(a)	2174	1.13×10^{-17}	1549	6.59×10^{-18}	GeH_3 asymmetric stretch
ν_3(a)	2152	1.13×10^{-17}	1527	5.53×10^{-18}	GeH_3 symmetric stretch
ν_4(a)	1908	4.83×10^{-17}	1359	2.47×10^{-17}	GeH_2 asym. strech
ν_5(a)	1886	4.13×10^{-17}	1342	2.07×10^{-17}	GeH_2 sym. strech
ν_6(a)	1680	4.36×10^{-17}	1194	2.28×10^{-17}	H–GeH_3 strech
ν_7(a)	1097	6.44×10^{-18}	780	3.30×10^{-18}	Ge···H–Ge bend
ν_8(a)	918	8.51×10^{-18}	653	4.41×10^{-18}	GeH_2 bend
ν_9(a)	892	2.41×10^{-18}	633	1.31×10^{-18}	GeH_3 deformation
ν_{10}(a)	876	7.89×10^{-18}	624	4.03×10^{-18}	GeH_3 deformation
ν_{11}(a)	816	9.36×10^{-18}	583	4.73×10^{-18}	Deformation
ν_{12}(a)	782	5.16×10^{-17}	562	2.62×10^{-17}	GeH_3 umbrella
ν_{13}(a)	566	5.36×10^{-18}	409	3.21×10^{-18}	GeH_2 rock
ν_{14}(a)	545	1.69×10^{-18}	391	6.27×10^{-19}	GeH_2, GeH_3 torsion
ν_{15}(a)	397	3.07×10^{-18}	286	1.50×10^{-18}	H–GeH_3 rock
ν_{16}(a)	208	1.44×10^{-19}	148	6.69×10^{-20}	Torsion
ν_{17}(a)	104	2.44×10^{-20}	73	1.48×10^{-20}	Torsion
ν_{18}(a)	93	9.41×10^{-20}	90	9.07×10^{-20}	Ge···Ge strech
	Ge_2H_5(a)		Ge_2D_5(a)		$H_3GeGeH_2(X^2A')$
$\nu_1(a')$	2135	1.59×10^{-17}	1519	9.02×10^{-18}	GeH_3 asymmetric stretch
$\nu_2(a')$	2105	1.63×10^{-17}	1495	7.70×10^{-18}	GeH_3 symmetric stretch
$\nu_3(a')$	2073	1.95×10^{-17}	1472	1.02×10^{-17}	GeH_2 sym. strech
$\nu_4(a')$	887	7.54×10^{-18}	631	4.02×10^{-18}	GeH_3 deformation
$\nu_5(a')$	863	2.46×10^{-18}	616	8.21×10^{-19}	GeH_2 bend
$\nu_6(a')$	786	6.33×10^{-17}	564	3.28×10^{-17}	GeH_3 umbrella
$\nu_7(a')$	555	4.29×10^{-18}	406	2.27×10^{-18}	Rock
$\nu_8(a')$	388	2.51×10^{-18}	277	1.24×10^{-18}	Rock
$\nu_9(a')$	246	3.06×10^{-20}	243	3.77×10^{-20}	Ge–Ge stretch
$\nu_{10}(a'')$	2143	2.48×10^{-17}	1528	1.33×10^{-17}	GeH_3 asymmetric stretch
$\nu_{11}(a'')$	2103	1.81×10^{-17}	1500	8.88×10^{-18}	GeH_2 asym. strech
$\nu_{12}(a'')$	888	5.55×10^{-18}	631	2.83×10^{-18}	GeH_3 deformation
$\nu_{13}(a'')$	566	1.18×10^{-19}	413	6.03×10^{-20}	Rock
$\nu_{14}(a'')$	371	2.46×10^{-18}	263	1.23×10^{-18}	Rock
$\nu_{15}(a'')$	113	3.61×10^{-20}	80	1.77×10^{-20}	Torsion
	Ge_2H_5 (b)		Ge_2D_5 (b)		$H_3GeH\cdots GeH$ (X^1A)
ν_1(a)	2182	1.02×10^{-17}	1556	5.86×10^{-18}	GeH_3 asymmetric stretch
ν_2(a)	2169	1.05×10^{-17}	1545	6.17×10^{-18}	GeH_3 asymmetric stretch
ν_3(a)	2143	1.16×10^{-17}	1521	5.73×10^{-18}	GeH_3 sym. strech
ν_4(a)	1849	5.06×10^{-17}	1317	2.55×10^{-17}	GeH strech
ν_5(a)	1750	4.49×10^{-17}	1244	2.34×10^{-17}	Ge–H···Ge strech
ν_6(a)	1048	9.33×10^{-18}	745	4.78×10^{-18}	GeH···Ge bend
ν_7(a)	884	3.87×10^{-18}	628	2.16×10^{-18}	GeH_3 deformation
ν_8(a)	869	9.62×10^{-18}	620	4.80×10^{-18}	GeH_3 deformation
ν_9(a)	782	4.45×10^{-17}	563	2.27×10^{-17}	GeH_3 umbrella
ν_{10}(a)	741	1.88×10^{-17}	530	9.66×10^{-18}	GeH_3 umbrella
ν_{11}(a)	562	4.96×10^{-18}	405	2.66×10^{-18}	GeH bend
ν_{12}(a)	373	2.28×10^{-18}	269	1.16×10^{-18}	GeH_4 rock

(*continued on next page*)

Table 3 (*continued*)

Modes	Frequencies	Intensities	Frequencies	Intensities	Characterization
ν_{13}(a)	167	1.25×10^{-19}	120	5.63×10^{-20}	Torsion
ν_{14}(a)	83	5.62×10^{-20}	77	5.66×10^{-20}	GeH_4 rock
ν_{15}(a)	58	3.90×10^{-20}	42	1.73×10^{-20}	GeH_4 rotation

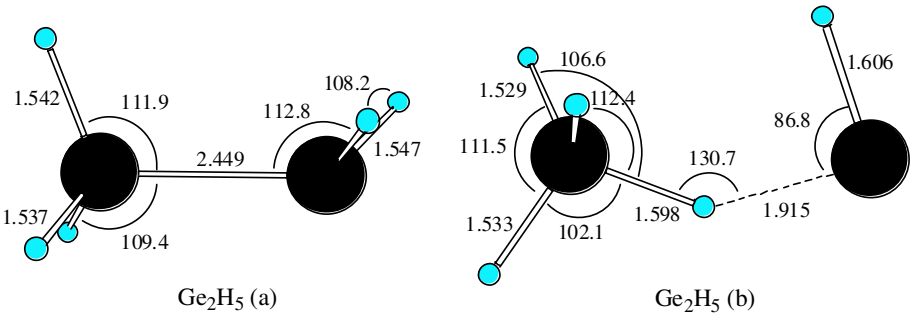

Fig. 3. Two isomeric structures of Ge_2H_5 calculated with the B3LYP/6-311G(d,p) method. Bond lengths and bond angles are in Å and °.

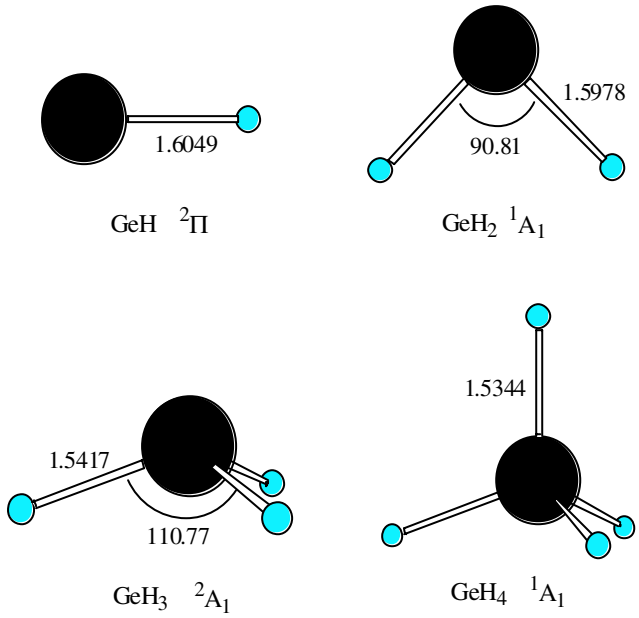

Fig. 4. Optimized structures of the ground state of GeH_x ($x = 1$–4) calculated with the B3LYP/6-311G(d,p) method. The bond length and bond angles are in Å and °.

of 0.97 – a sensible value for the B3LYP/6-311G (d,p) level of theory – this data compares nicely with the ν_6 mode of the hitherto elusive digermyl radical, $Ge_2H_5(X^2A')$. This absorption has the highest integral absorption coefficient of all the fundamentals of the digermyl radical (Table 3). Note that the ν_1–ν_3 and ν_{10}–ν_{11} absorptions of the digermyl radical are blocked by the strong absorption of the ν_3 peak of the germane matrix. The integral absorption coefficients of the remaining fundamentals of $Ge_2H_5(X^2A')$ are about one order of magnitude lower than of the ν_6 mode, and we do not expect to monitor these vibrations. To verify our conclusions and hence the detection of the germyl radicals, we also probed the exposure of the d4-germane matrix to a larger electron current. Here, two additional features developed in time. These are located at 561 cm^{-1} and 616 cm^{-1}. These absorptions agree nicely with the scaled, computed ν_6 and ν_4/ν_{12} modes of the d5-digermyl radical. Also, the corresponding ν_1–ν_3 and ν_{10}–ν_{11} transitions are obscured by ν_3 mode of the d4-germyl matrix; all fundamentals having absorptions lower than 500 cm^{-1} cannot be observed due to the cutoff of our FT-IR detector. The integrated absorption coefficient of the only remaining absorption of the d5-digermyl radical (ν_5) is a factor of 4–5 lower than those of the detected ν_6 and ν_4/ν_{12} modes and, hence, is too low to be detected. We also would like to emphasize that we did not observe any absorption of the energetically unfavorable H_3GeH–GeH isomer (Fig. 2; Table 1) suggesting that the germanium-germanium bond is not cleaved during the fragmentation of the digermane molecule.

6. Discussion and summary

The infrared and mass spectroscopic data imply that the response of the germane ices upon the electron irradiation is governed by an initial germane–hydrogen single bond rupture which forms atomic hydrogen plus the germyl radical, $GeH_3(X^2A_1)$, Eq. (10). In order to escape the $[GeH_3 \cdots H]$ matrix cage, the hydrogen atom needs an excess energy – the lattice binding energy – of a few tens of kJ mol^{-1} to escape [45]. Otherwise, atomic hydrogen will recombine with the germyl radical to react back to a germane molecule. Our mass spectrometric data verify the formation of mobile hydrogen atoms in the germane matrix. An increase of the ion current of $m/e = 2$ (H_2) is evident (Fig. 10). Recall that we did not identify any absorptions of any GeH_x or GeD_x ($x = 1$, 2) species in the solid matrices; hence we can deduce that the molecular hydrogen is formed via recombination of two hydrogen atoms in the matrix (reaction (13)). We would like

Table 4
Unscaled vibrational frequencies (cm^{-1}) and infrared intensities (cm $molecule^{-1}$) calculated with B3LYP/6-311G(d,p) level of theory

Mode		Frequency	Intensity	Frequency	Intensity
		GeH ($X^2\Pi$)		GeD ($X^2\Pi$)	
ν_1	σ	1854	6.27×10^{-17}	1320	3.18×10^{-17}
		$GeH_2(X^1A_1)$		$GeD_2(X^1A_1)$	
ν_1	a_1	1883	5.31×10^{-17}	673	5.25×10^{-18}
ν_2	a_1	945	1.06×10^{-17}	1340	2.73×10^{-17}
ν_3	b_2	1889	5.95×10^{-17}	1345	3.02×10^{-17}
		$GeH_3(X^2A_1)$		$GeD_3(X^2A_1)$	
ν_1	a	2076	1.66×10^{-18}	1470	8.78×10^{-19}
ν_2	a	714	9.00×10^{-18}	514	4.67×10^{-18}
ν_3	e	2123	2.51×10^{-17}	1515	2.62×10^{-17}
ν_4	e	861	9.08×10^{-18}	614	9.13×10^{-18}
		$GeH_4(X^1A_1)$		$GeD_4(X^1A_1)$	
ν_1	a_1	2128	0	1506	0
ν_2	e	926	0	655	0
ν_3	t_2	2135	2.11×10^{-17}	1522	3.39×10^{-17}
ν_4	t_2	822	1.85×10^{-17}	592	2.85×10^{-17}

Table 5
Newly observed species and their absorptions in low temperature germane matrices

Species	Frequency (cm^{-1})	Fundamental	Species	Frequency (cm^{-1})	Fundamental
GeH_3	665	ν_2	GeD_3	608	ν_4
Ge_2H_6	870	ν_{11}	Ge_2D_6	626	ν_{11}
	752	ν_6		529	ν_6
Ge_2H_5	765	ν_6	Ge_2D_5	616	ν_4/ν_{12}
				561	ν_6

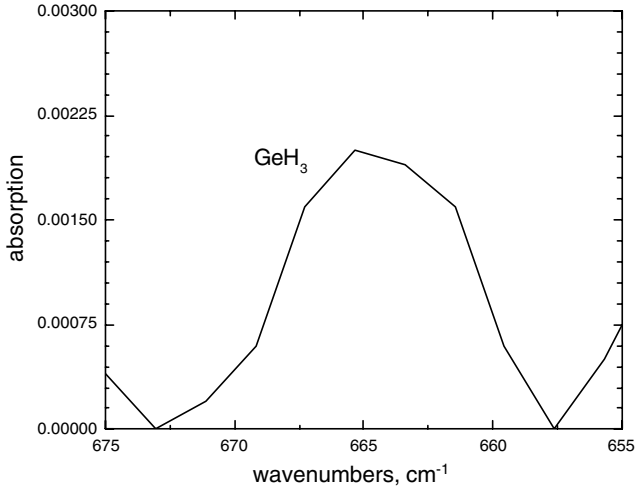

Fig. 5. New absorption feature of the germyl radical, $GeH_3(X^2A_1)$, at 665 cm^{-1} in the germane matrix at 12 K.

to emphasize that $m/e = 2$ is the only signal detected with the mass spectrometer during the irradiation of the germane matrix at 12 K (Fig. 10). None of the GeH_x ($x = 2$–4) species was found in the gas phase during the irradiation phase. This clearly demonstrates that $m/e = 2$ is not a fragment from germane hydride species in the gas phase.

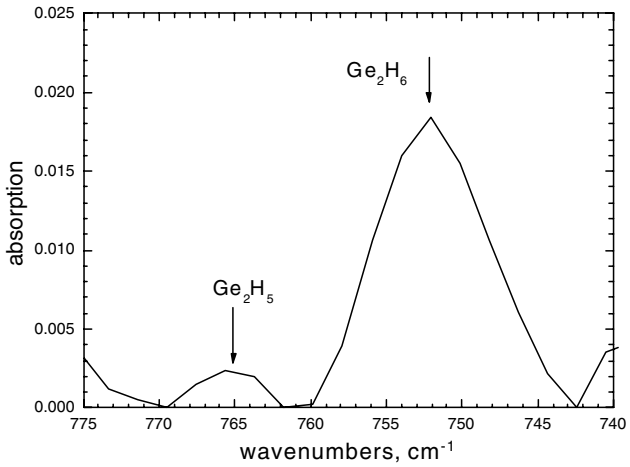

Fig. 6. New absorption features of the digermane molecule, Ge_2H_6-(X^1A_{1g}) at 752 cm^{-1}, and of the digermyl radical, $Ge_2H_5(X^2A')$ at 765 cm^{-1}, in the germane matrix at 12 K.

$$H(^2S_{1/2}) + H(^2S_{1/2}) \rightarrow H_2(X^1\Sigma_g^+) \quad (13)$$

We would like to comment now on the formation mechanism of the digermane molecule. The infrared data suggest that the digermane molecule is formed initially within a single trajectory of the electron. It is important to note that in strong contrast to photons, each electron can release its kinetic energy via multiple energy transfers to various germane molecules. Utilizing the CASINO code [46], we find that each 5 keV electron loses 0.20 ± 0.02 keV of its kinetic energy while penetrating the germane target; this corresponds to an averaged electronic energy transfer of 4.0 ± 0.4 keV μm^{-1}. Since the dissociation energy of the Ge–H bond has been determined to be 350 ± 8 kJ mol^{-1} (3.62 eV) [47,48], we can conclude that each electron can generate up to 55 germyl radicals in the matrix. Considering the unit cell of a germane crystal [21], about one germyl radical is generated on average per unit cell. Here,

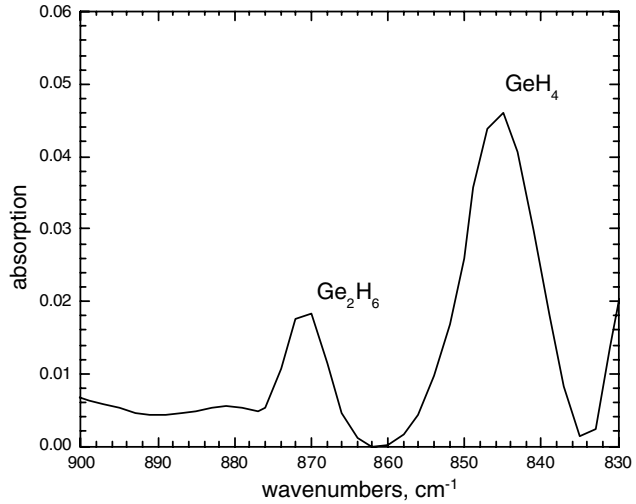

Fig. 7. New absorption features of the digermane molecule, Ge_2H_6-(X^1A_{1g}) at 870 cm^{-1} in the germane matrix at 12 K.

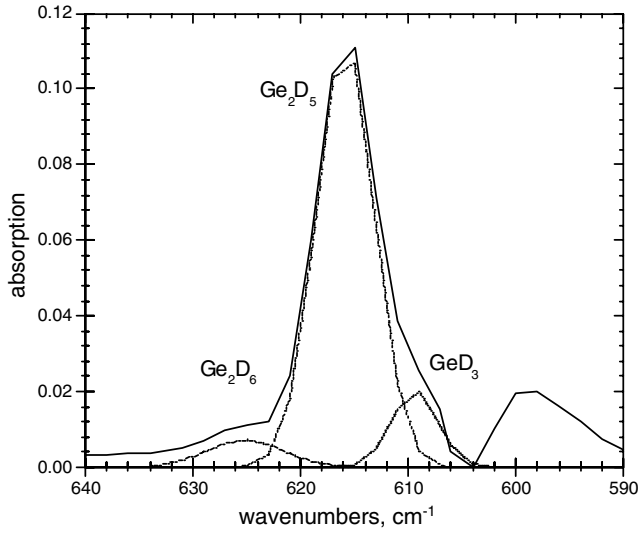

Fig. 8. New absorption features of the d3-germyl radical $GeD_3(X^2A_1)$ at 608 cm^{-1}, d6-digermane molecule, $Ge_2D_6(X^1A_{1g})$ at 626 cm^{-1}, and of the d5-digermyl radical, $Ge_2D_5(X^2A')$ at 616 cm^{-1}, in the d4-germane matrix at 12 K.

neighboring germyl radical can recombine to the digermane molecule $Ge_2H_6(X^1A_{1g})$ at 12 K if they have the correct recombination geometry. A diffusion-limited reaction mechanism of the germyl radical, can be ruled out since our infrared data suggest that within the isothermal 12 K phase, the column density of the germyl radical is constant; this verifies that the germyl radical is immobile at 12 K. We would like to stress that in principle suprathermal hydrogen atoms can also abstract a hydrogen atom form a germane molecule to form molecular hydrogen plus a germyl radical. Finally, we investigated the temporal evolution of the column densities of the digermane molecule and of the digermyl radical (Fig. 11). These profiles of the column densities of the digermane and digermyl radicals were fit with a sequential reaction mechanism $A \rightarrow B \rightarrow C$

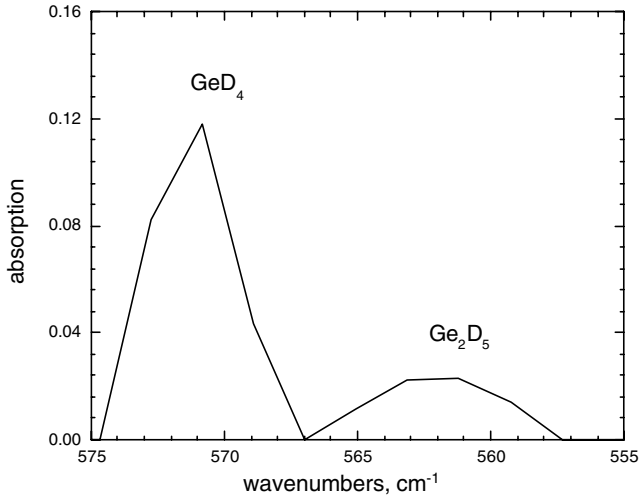

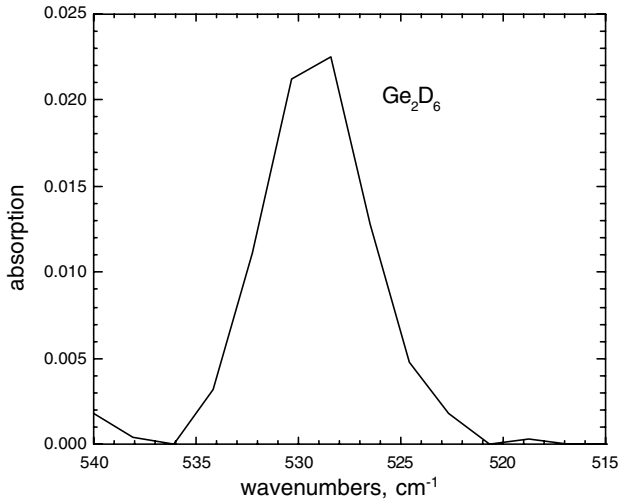

Fig. 9. New absorption features of the d5-digermyl radical, $Ge_2D_5(X^2A')$ at 561 cm^{-1} and the d6-digermane molecule, $Ge_2D_6(X^1A_{1g})$ at 529 cm^{-1}, and of the in the d4-germane matrix at 12 K.

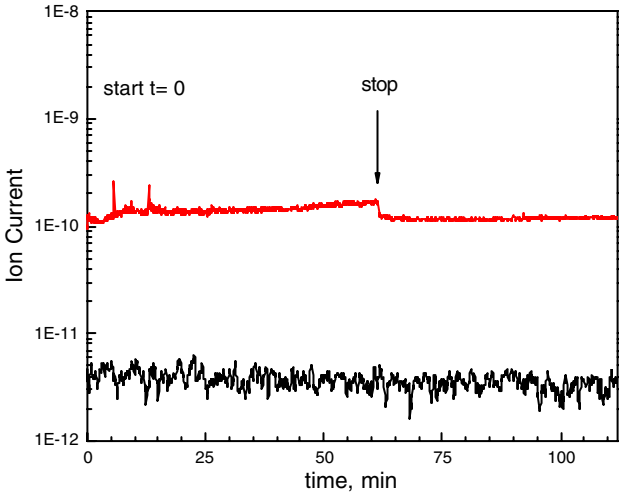

Fig. 10. Temporal profile of the germane ($m/e = 77$; bottom) and molecular hydrogen ($m/e = 2$; top) evolution during the irradiation (start-stop) and the isothermal phases at 12 K of the germane matrix.

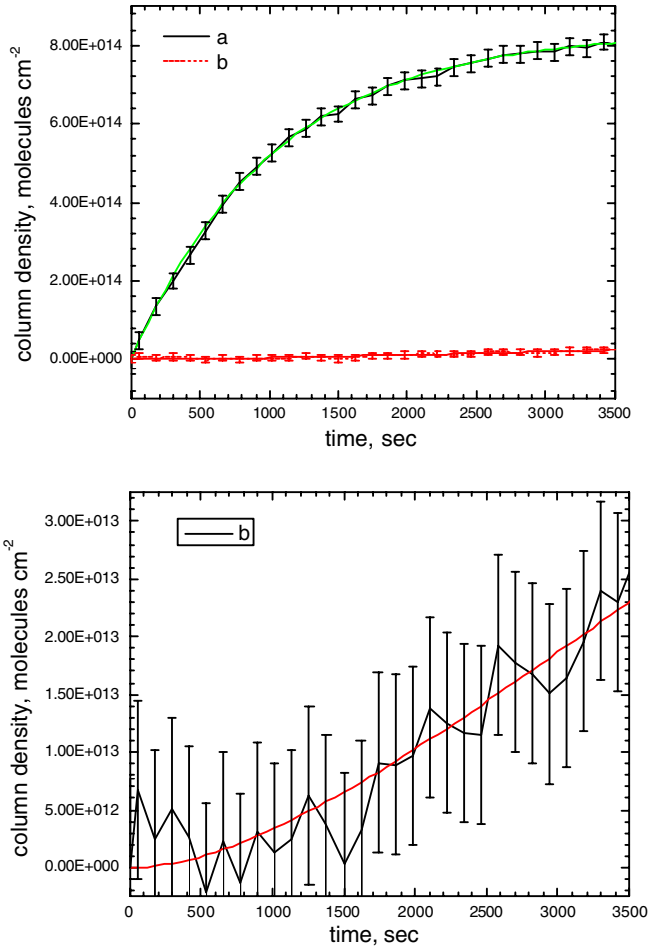

Fig. 11. Temporal evolution of the experimental column densities and the best fits of the digermane (a) and digermyl radicals (b) during the irradiation of the germane matrix at 12 K.

utilizing Eqs. (14) and (15) [49]. Here, A presents formally a germane dimer, B the digermane molecule and two hydrogen atoms and/or a hydrogen molecule, and C the digermyl radical plus atomic hydrogen formed via an electron induced decomposition of the digermane molecule. This procedure yields best fits with $b = 2.7 \pm 0.2 \times 10^{16}$ molecules cm^{-2}, $k_1 = 9.7 \pm 0.4 \times 10^{-4}$ s^{-1}, and $k_2 = 3.4 \pm 0.3 \times 10^{-7}$ s^{-1}. These data confirm quantitatively that the digermyl radical is indeed a decomposition product of the digermane molecule.

$$[Ge_2H_6](t) = \frac{k_1 b}{k_2 - k_1}\left(e^{-k_1 t} - e^{-k_2 t}\right) \quad (14)$$

$$[Ge_2H_5](t) = b\left[1 - \frac{k_2}{k_2 - k_1}e^{-k_1 t} + \frac{k_1}{k_2 - k_1}e^{-k_2 t}\right] \quad (15)$$

Summarized, the digermyl, $Ge_2H_5(X^2A')$ and d5-digermyl, $Ge_2D_5(X^2A')$, radicals were detected in germane and d4-germane matrices at 12 K via infrared spectroscopy. The ab initio calculations showed that the most intense absorption of the digermyl radical should be observable for the ν_6 fundamental at 770 cm^{-1} $Ge_2H_5(X^2A')$ and 547 cm^{-1} $Ge_2D_5(X^2A')$, respectively. The experimental results (765 cm^{-1} and 561 cm^{-1}) are in good agreement with the computed data. These data help in the monitoring of time resolved infrared spectroscopy of germane CVD processes and can also guide prospective observations of germanium-bearing molecules in the atmospheres of Jupiter and Saturn in the infrared regime to better understand the chemical evolution of planetary atmospheres under extreme environments.

Acknowledgements

The experiments were supported by the NASA Space Grant administered by the University of Hawai'i at Manoa (W.C.) and by the NASA Astrobiology Institute under Cooperative Agreement NNA04 CC08A at the University of Hawaii-Manoa (W.Z., R.I.K.). The computations were carried out at the computer center of the Institute for Molecular Science, Japan, and supported by the Grants-in-Aid for Scientific Research on Priority Areas from the Ministry of Education, Science, and Culture, Japan (Y.O.).

References

[1] A. Ricca, C.W. Bauschlicher, J. Phys. Chem. A (1999) 11121.
[2] P.A. Cook, M.N.R. Ashfold, Y.-J. Jee, K.-H. Jung, S. Ha, X. Yang, Phys. Chem. Chem. Phys. 3 (2001) 1848.
[3] S.D. Chambreau, J. Zhang, Chem. Phys. Lett. 351 (2002) 171.
[4] H. Kim, J.E. Greene, Surf. Sci. 504 (2002) 108.
[5] O. Dag, A. Kuperman, G.A. Ozin, Symp. Proc. 358 (1995) 87.
[6] Special Issue 'Nanostructure', Chem. Rev. 99 (1999).
[7] Special Issue 'Surface Chemistry – Advances and Technological Impact', Chem. Rev. 96 (1996).
[8] J. Perrin, M. Shiratani, P. Kae-Nune, H. Videlot, J. Jolly, J. Guillon, J. Vac. Sci. Technol. (1998) 278.
[9] J.G.E. Gardeniers, L.J. Giling, F.D. Jong, J.P. van der Eerden, J. Crystal Growth 104 (1990) 727.
[10] Q.-S. Li, R.-H. Lu, Y. Xie, H.F. Schaefer III, J. Comput. Chem. 23 (2002) 1642.
[11] Z.-X. Wang, M.B. Haung, J. Chem. Soc., Faraday Trans. 94 (1998) 635.
[12] S. Oikawa, M. Tsuda, S. Ohtsuka, J. Mol. Struct. (THEOCHEM) 116 (1994) 287.
[13] B. Ruscic, J. Berkowitz, J. Chem. Phys. 95 (1991) 2416.
[14] V.A. Crawford, K.H. Rhee, M.K. Wilson, J. Chem. Phys. 37 (1962) 2377.
[15] X. Wang, L. Andrews, G.P. Kushto, J. Phys. Chem. A 106 (2002) 5809.
[16] J. Urban, P.R. Schreiner, G. Vacek, Pv.R. Schleyer, J.Q. Huang, J. Leszczynski, Chem. Phys. Lett. 264 (1997) 441.
[17] X. Wang, L. Andrews, J. Am. Chem. Soc. 125 (2003) 6581.
[18] C.J. Bennett, C.S. Jamieson, Astrophys. J (2006) submitted for publication.
[19] D. Sillars, C.J. Bennett, Y. Osamura, R.I. Kaiser, Chem. Phys. Lett. 392 (2004) 541.
[20] D. Sillars, C. Bennett, R.I. Kaiser, Y. Osamura, Chem. Phys. Lett. (2004).
[21] P. Calvani, C. Ciotti, A. Cunsolo, S. Lupi, Solid State Commun. 75 (1990) 189.
[22] P. Calvani, S. Lupi, C. Ciotti, J. Chem. Phys. 94 (1991) 52.
[23] D.C. McKean, A.A. Chalmers, Spectrochim. Acta A 23 (1967) 777.
[24] S.K. Atreya, M.H. Wong, T.C. Owen, P.R. Mahaffy, H.B. Niemann, I.D. Pater, P. Drossart, T. Encrenaz, Planet. Space Sci. 47 (1999) 1243.
[25] A.J. Bridgemanm, L.R. Ireland, Polyhedron 20 (2001) 2841.
[27] H. Gruetzmacher, T. Faessler, Chem. Eur. J. 6 (2001).

[28] H.J. Himmel, H. Schnoeckel, Chem. Eur. J. 8 (2002).
[29] V.N. Khabashesku, S.E. Boganov, K.N. Kudin, J.L. Margrave, J. Michl, O. Nefedov, Russ. Chem. Bull. (Translation of Izvestiya Akademii Nauk, Seriya Khimicheskaya) 48 (1999) 2003.
[30] W.C. Chen, M.D. Su, S.Y. Chu, Organometallics 20 (2001).
[31] H. Jacobsen, T. Ziegler, J. Am. Chem. Soc. 116 (1994) 3667.
[33] A.M. Coats, D.C. McKean, D. Steele, J. Mol. Struct. 320 (1993) 269.
[35] D.C. McKean, I. Torto, M.W. Mackenzie, A.R. Morrisson, Spectrochim. Acta A 39 (1983) 387.
[36] A.D. Becke, J. Chem. Phys. 98 (1993) 5648.
[37] C. Lee, W. Yang, R.G. Parr, Phys. Rev. B 37 (1988) 785.
[38] R. Krishnan, J.S. Binkley, R. Seeger, J.A. Pople, Chem. Phys. 72 (1980) 650.
[39] J. Cizek, Adv. Chem. Phys. 14 (1969) 35.
[40] J.A. Pople, M. Head-Gordon, K. Raghavachari, J. Chem. Phys. 87 (1987) 5968.
[41] R.A. Kendall, T.H. Dunning, R.J. Harrison, J. Chem. Phys. 96 (1992) 6796.
[42] M.J. Frisch et al., GAUSSIAN-98, Revision A11, 2002.
[45] R.I. Kaiser, G. Eich, A. Gabrysch, K. Roessler, Astrophys. J. 484 (1997) 487.
[46] D. Drouin, P. Hovington, R. Gauvin, Scanning 19 (1997) 1.
[47] M.B. Coolidge, W.T. Bordon, J. Am. Chem. Soc 110 (1988) 2298.
[48] W. Thiel, A.A. Voityuk, J. Mol. Struct. (THEOCHEM) 313 (1994) 141.
[49] J.I. Steinfeld, J.S. Francisco, W.L. Hase, Chem. Kinet. Dynam. (1999).